# Probing Dynamically Tunable Localized Surface Plasmon Resonances of Film-Coupled Nanoparticles by Evanescent Wave Excitation

*Jack J. Mock[1, 2], Ryan T. Hill[3], Yu-Ju Tsai[1, 2], Ashutosh Chilkoti[3, 4], David R. Smith[1,2*]*

[1]Department of Electrical and Computer Engineering, Duke University, Durham, NC

[2]Center for Metamaterials and Integrated Plasmonics, Duke University, Durham, NC

[3]Center for Biologically Inspired Materials and Material Systems, Duke University, Durham, NC

[4]Department of Biomedical Engineering, Duke University, Durham, NC

[*]To whom correspondence should be addressed. Email: drsmith@ee.duke.edu

# Supporting Information

## Gold NP- Gold Film Sample Preparation

Gold films and polyelectrolyte (PE) spacer layers were prepared and characterized as described previously (*1*). Briefly, 30 nm gold films were deposited by an electron beam evaporator (CHA Industries) at 2 Angstroms/sec onto clean room cleaned Nexterion Glass B slides (Schott North America, Inc.) using a 5 nm chromium adhesion layer (deposited at 1 Angstrom/sec). Layer-by-layer (LBL) deposition (*2*) of poly (allylamine) hydrochloride (PAH, $M_w$ = 70 kDa, Aldrich) and polystyrene sulfonate (PSS, $M_w$ = 70 kDa, Aldrich) was used to create PE spacer layers. For each deposition step, the gold-coated glass slides were immersed in 0.003 moles-of-monomer/L (monomol/L) PE and 1 M NaCl for 30 min, rinsed thoroughly with a gentle stream of ultra-pure water (18 MΩ, used throughout), and immersed in fresh ultra-pure water for 1 min, after which the substrates were either immersed in 1 M NaCl for 30 s before repeating the same steps for deposition of the oppositely charged PE or dried with a stream of high-purity nitrogen for analysis. All LBL depositions were initiated and terminated with the cationic PAH layer to facilitate both the attachment of the first PE layer to the gold film through amine-gold interactions (*3*) and the electrostatic immobilization of gold nanoparticles to the PE spacer layer. A single PAH layer was utilized for most of the reported work.

Self-assembled monolayers (SAMs) of thiols on gold films were fabricated using 1mM of either 11-Amino-1-undecanethiol hydrochloride (Aldrich, referred to as “amine thiol” or “C11 amine thiol” in our text) or 2-{2-[2-(2-{2-[2-(1-mercaptoundec-11-yloxy)-ethoxy]-ethoxy}-ethoxy)-ethoxy]-ethoxy}-ethylamine hydrochloride (Prochimia, referred to as “C11 EG6 amine thiol” in our text) in absolute ethanol. The SAMs were fabricated by incubating a gold slide in a clean glass vial containing the thiol solution for 18 hours. Following the incubation, the vials were sonicated in a water bath at low power

for 2 minutes and then overflow rinsed with 5 reaction volumes of absolute ethanol. This sonication and rinsing step was performed a total of 4 times for each slide before removing the slide from the ethanol solution and drying it with a stream of high-purity nitrogen.

60nm gold NPs (BBI) were electrostatically immobilized on the top surfaces of each molecular spacer layer. Deposition of gold NPs was done by applying ~400-μL drops of gold colloid- un-diluted (1x), 1:5 dilution (0.2x), 1:10 dilution (0.1x) and 1:20 dilution (0.05x) with ultra-pure water- to each functionalized gold film for 30 minutes in a humidity chamber followed by rinsing with ultra-pure water and drying under a stream of nitrogen.

## Molecular Spacer Layer Thickness Measurements

Film-NP gap distances are assumed to be set by the molecular spacer thickness. Spacer layer thicknesses were measured using a J.A. Woolam Co., Inc., M-88 spectroscopic ellipsometer and WVASE32 software (version 3.460). Spectroscopic scans (277.5 – 763 nm) of each spacer layer were performed in three distinct regions (free of immobilized NPs) at 65°, 70°, and 75° relative to the normal of the surface of the slide. Ellipsometry data was analyzed using a 2-layer model (*4*) composed of a bulk gold layer underneath an organic layer, which was used to represent the molecular layer. The thickness of each spacer layer was fitted using the Cauchy expression for a normal dispersion (*5*), where parameters "A" and "B" were fitted such that the mean standard error of the fit was minimized. For each spacer layer, the nominal thickness was determined to be the average of the three thickness measurements taken per spacer layer. Note that the optical constants of each bare gold film were determined immediately prior to LBL depositions by taking spectroscopic scans of the bare gold films at 65°, 70°, and 75° and fitting $n$ and $k$ to the known values of bulk gold, which were provided by the WVASE32 software, to account for any shifts in the optical constants due to the thicknesses of our gold films. These fitted optical constants for each gold slide were saved and used later, respectively, when

fitting for thickness of the molecular layers deposited onto the gold slides. Measured PE spacer thickness versus film-coupled NP LSPR for the 'dry' sample is plotted in Figure 2B.

## Angle Dependence of the T.I.R. Reflectivity and Discrimination of LSPR from SPR

Figure I

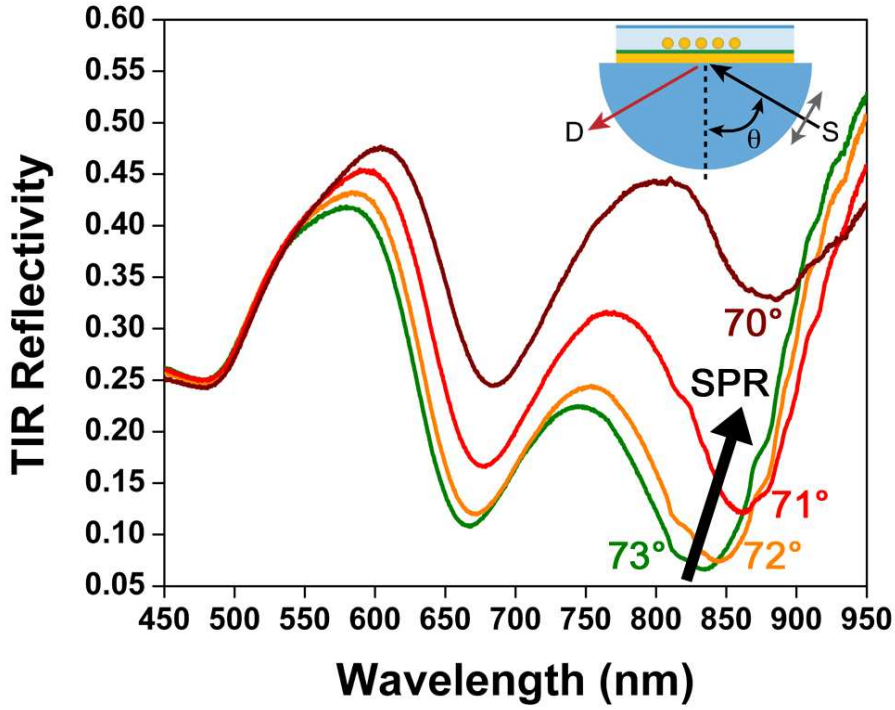


Under evanescent field excitation, the LSPR of the NPs and the delocalized SPR of the gold film are influenced by each other. The LSPR of each individual NP is red-shifted and polarized by the gold film, while the evanescent field—which excites the NPs—also couples to the SPR of the gold film; thus, the spectrum of the excitation field represents a convolution of the incident light and the SPR. Likewise, the SPR of the gold film is red-shifted by the higher surface coverage of the NPs. While the presence of the two extinction dips is a promising sign for LSPR characterization using TIR reflectivity, at the wrong incidence angle it would initially appear that the two resonances are perhaps too entangled for an unambiguous measurement of the pure LSPR response. However, it is possible to spectrally detangle the localized film-NP response from the delocalized SPR of the film by simply changing the angle of TIR illumination. In Figure I, again using the sample prepared 1x NP concentration and using a single PAH

spacer layer, we show that by decreasing the angle of the incident white light illumination from 73° to 70° (inset: experimental geometry), we can red-shift the SPR of the gold film and reveal a more distinct LSPR from the film-NPs. This is possible because each film-NP resonance is localized to a sub-wavelength single dipolar structure, so it does not have the same angle dependence as the SPR from the planar gold film. The efficiency of excitation of the film-NPs can be improved by adjusting the angle to maximize the illumination polarization component parallel to the vertical dipole, but the fundamental resonance remains fixed. However, changing the angle of illumination changes the momentum vector of the evanescent field and directly alters the select SPR modes that this field will couple to. Once the LSPR is spectrally separated from the SPR signal, for example at 70°, it becomes easier to clearly resolve the LSPR shifts associated with changes in the film-NPs average gap dimension.

**Power Law Gap-Distance Dependence of LSPR**

Figure II

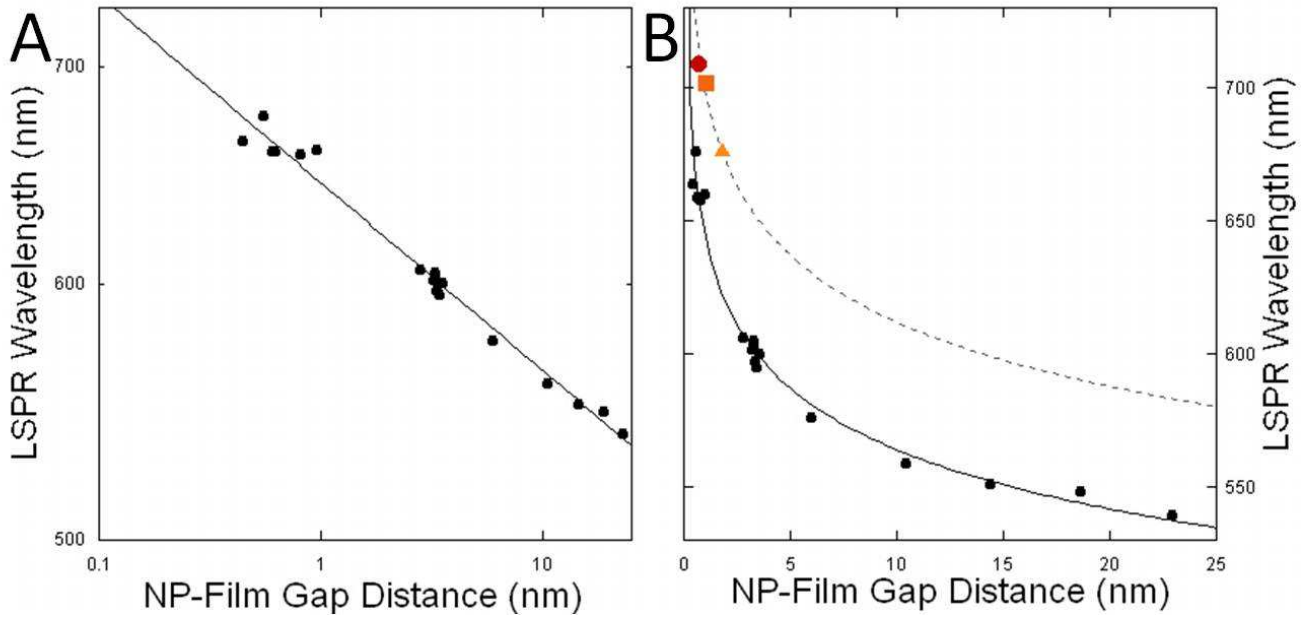


Shown in Figure II A is the LSPR Peak position plotted versus the film-NP gap distance (poly-electrolyte spacer layers- same data as Figure 2B) on a log-log scale. Guided by a recent article from

Baumberg et al (*6*), we have fit this data with a power law function ($y = 644.43 * d^{-0.058}$, R=.99147, d= gap dimension, y = LSPR wavelength). While the linear appearance of the data on the log scale is a signature of the power law function, this relationship is not sufficient to determine that the system will obey the power law in the asymptotic limit where the film-NP gap distance approaches zero. It is interesting to discover that the LSPR spectra from the smallest film-coupled NP gap presented in this article (1 PAH layer, ~5 Angstroms) continues to obey the power law, but we expect that at some smaller gap dimension the rule will break down.

In this article, we use the power law relationship between the gap dimension and the LSPR position to make a very rough estimate of the NP displacement from the LSPR shift observed during application of an electric field across the flow cell. However, a correction factor must be applied to the power law fit in Figure II (superstrate = air, standard reflectivity measurements) before it can be used in conjunction with the data acquired for the fluid immersed film-coupled NPs (superstrate = water, TIR reflectivity measurements). We cannot directly measure the spacer layer thickness in water due to ellipsometer instrument limitations, and we are not currently equipped to capture the LSPR scattering spectra from the film-NPs in water. In Figure II B we graphically demonstrate how we convert the gap dimension dependence of the LSPR which has been directly measured (solid line), to the predicted relationship under immersion in the flow cell geometry (dashed grey line). For each film-NPs sample prepared for TIR characterization, we pre-measure the molecular spacer layer thickness 'dry' using the ellipsometer and for the PAH layer we assume that a 40% swelling occurs from layer hydration effects during buffer immersion (*7-10*). We note that this swelling factor is highly subjective, and there is no way to determine its exact value. The film-NPs sample used for the data presented in Figure 5 had a measured 'dry' average thickness of 18.28 Angstroms for the C11 EG6 amine thiol layer, 10.13 Angstroms for the C11 amine thiol layer and 5.08 Angstroms for the PAH film (giving the PAH an estimated hydrated thickness of 7.11 Angstroms). We then determine the initial LSPR peak position (using the centroid calculation) from the TIR reflectivity measurement of our flow-cell-modified sample with the surface immersed in the buffer and under 0 Volts electric field applied. This wavelength was determined to be

676.5nm (C11 EG6 amine thiol), 701.5nm (C11 amine thiol) and 709.2nm (PAH) at the beginning of measurements for the samples presented in Figure 5. Once the film thickness and LSPR position are known for each of these samples, we plot these points [Triangle - (1.828, 676.5), Square – (1.013, 701.5), Circle - (0.711, 709.19)] on the graph in Figure II B. By imposing a linear vertical offset correction factor, which effectively equates to a 55nm red-shift, to the 'dry' PAH samples' power law curve fit (solid line), we force the new curve ($y = 699.43 * d^{-0.058}$, y = LSPR wavelength) through the median of these 'wet' data points (dashed line). The red-shift is generally consistent with film-NPs immersion in a higher index of refraction medium. The new curve is now used to estimate the gap dimension (d) from the TIR measured LSPR position of the buffer immersed film-NPs as they are subject to electrophoretic forces.

**Response of the Delocalized Plasmon Resonance Peak to Applied Field**

Figure III

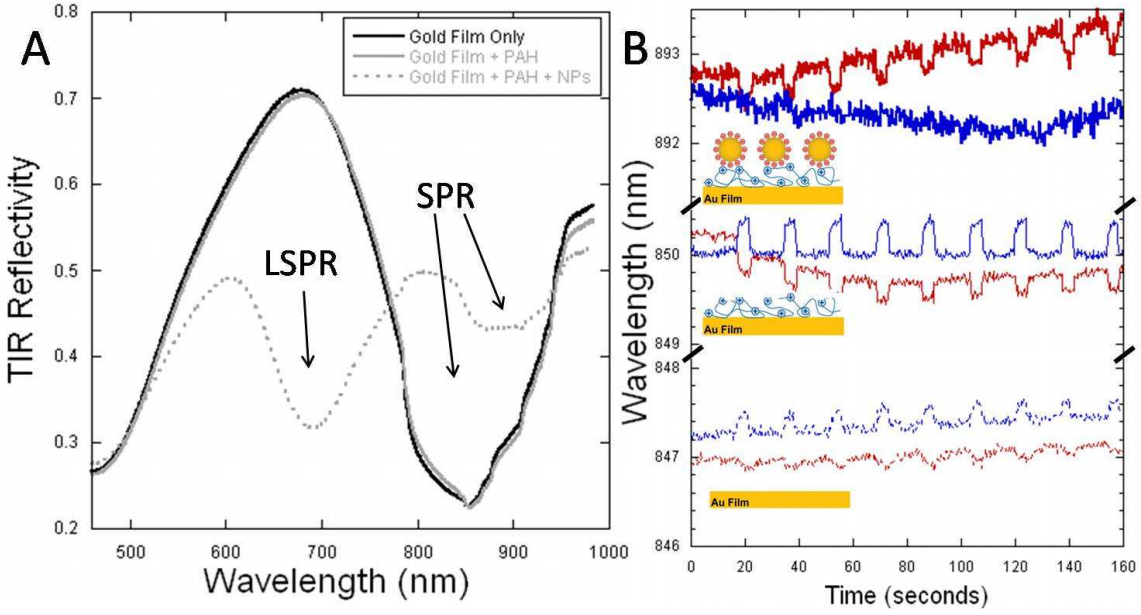


Shown in Figure III A are the TIR reflectivity curves from the bare 30nm gold film (solid black line), gold film with a single PAH layer (solid gray line), and gold film with a single PAH layer and NPs (dashed gray line). Only the sample with NPs has a resonance associated with the film-coupled NP

LSPR. All three samples display an extinction band from evanescent coupling to the delocalized SPR of the film. The position of the bare gold film SPR (around 850nm) is red-shifted slightly by addition of a single (~6 Angstrom) PAH layer and red-shifted dramatically by additional deposition of 60nm NPs at 1x concentration (~2.2% surface coverage). These red-shifts are consistent with increasing the refractive index of the region directly above the gold film. In Figure III B we plot the sequential series of the de-localised SPR peak positions (determined by centroid calculation) under pulses of 500mV DC applied electric field. The red curves correspond to the positive electrode at the top of the flow cell. The blue curves correspond to the negative electrode at the top of the flow cell. These TIR reflectivity measurements were made for bare gold film (bottom), gold film with a single PAH layer (middle), and for the gold film with NPs attached (1x concentration) to the single PAH layer (top). There is a small but measurable shift to the delocalized film resonance for all three samples when the electric field is applied. It is not clear what the root causes of these shifts are. In the case of the polymer layer, it can be suggested that there is some swelling associated with an applied field, which then causes a spectral shift of the SPR, but this cannot be the case for a bare film. Curiously, based on what we have reported for the LSPR, the SPR position of the gold film covered with NPs seems to be the least sensitive to the electric field. The surface effects resulting from applying a field between the gold film and the top of the flow cell are not well understood. There can be ionic charge build-up at the gold surface, heating, and even electrolysis, all of which may slightly affect the SPR wavelength which is very sensitive to surface changes.

**Plasmonic Characterization of Gold NPs near Gold Film**

Plasmon resonances of gold film-coupled NPs were characterized by single film-NP scattering spectra and color images (Fig. 1), ensemble-mode reflectivity spectra (Fig. 2, 3A), and ensemble-mode TIR reflectivity spectra (Fig. 3B-5). Single film-NP scattering spectra and color images were acquired as described previously (*1*). Briefly, film-NPs were imaged and their spectra taken using a customized Nikon darkfield (DF) microscope with a 100x DF 0.9 NA objective. Slides containing the gold films

with spacer layers and immobilized NPs were index-matched with oil to the top surface of a hemi-cylindrical lens which we use in place of a prism. Samples were illuminated from above using un-polarized white light from a 75 W Xenon lamp in DF mode. For color images, the microscope light path was directed to a Nikon d90 color camera. Film-NP spectra were acquired using a 200 μm image plane pinhole aperture to reduce the field of view to that of a single film-NP, or for the case of higher concentrations, smaller groups of film-NPs, which greatly reduces the background signal in the imaging path. This field of view was directed through a spectrometer (Acton 2300SPI) and onto a detector (Photometrics CoolSnap HQ). All DF spectra were background corrected (by subtracting the spectrum from an apertured region of the substrate containing no film-NPs) and normalized (by dividing the spectrum from a white scattering standard [Labsphere]) to correct for the wavelength response of the imaging system. Figure 1 shows representative spectra from single film-NPs and from clusters of film-NPs for high concentration preparations.

Reflectivity measurements from gold film-coupled NPs (Fig. 2, 3A) were made using the same lamp and collection spectrometer as DF scatter measurements. However, instead of collecting film-NP scattered light through the microscope, 1mm diameter multimode fibers fitted with fiber collimators are positioned to illuminate and collect the light reflected off the surface of the sample. A single linear polarizer is positioned at the output of the illumination fiber to provide P-polarization. The collection fiber is directed to and refocused at the entrance slit of the Acton Spectrometer. Spectra are normalized to a bare gold film. The lamp intensity must be reduced, using ND filters or aperture, by orders of magnitude to prevent saturation of the CCD detector. S-polarized light was also acquired (data not shown), but the response from the film-NPs for this orientation was too weak to measure. The reflectivity spectra represent the ratio of reflectivity from a spot on the gold film containing a PE spacer and many immobilized NPs to that of a spot on the gold film containing only the PE spacer layer. For this reason, the reflectivity measured resonances appear as dips in the plotted data, indicating that incident light reflected off the surface and directed at the detector is being both absorbed and scattered in all directions by the film-NPs. Extinction resonance peak positions were determined by finding the

centroid of the bottom 80% of each dip (Fig 2B). Amplitude of extinction was taken to be the minimum value from each of the extinction curves (Fig 2C).

TIR measurements were made using the same lamp and collection spectrometer as DF scatter measurements. However, instead of collecting film-NP scattered light through the microscope, 1mm diameter multimode fibers fitted with fiber collimators are positioned to illuminate and collect the light reflected off the underside of the sample through a hemi-cylindrical fused silica lens (Britek Laser Optic). A single linear polarizer is positioned at the output of the illumination fiber to provide P-polarization. Light incident in this manner enables the evanescent field to couple to both the LSPR of the gold film-coupled NPs and to select SPR modes of the gold film. The collection fiber is directed to and refocused at the entrance slit of the Acton Spectrometer. Spectra are normalized to a bare glass slide. The lamp intensity must be reduced, using ND filters or aperture, by orders of magnitude to prevent saturation of the CCD detector. To ensure consistent and reproducible detector performance, typical acquisition times for spectra were 200ms with a 100ms delay between sequential exposures.

**References**


1. (1) J. J. Mock *et al.*, Distance-dependent plasmon resonant coupling between a gold nanoparticle and gold film. *Nano Letters* **8**, 2245-2252 (2008).
2. G. Decher, Fuzzy nanoassemblies: toward layered polymeric multicomposites. *Science* **277**, 1232 (1997).
3. S. M. Marinakos, S. Chen, A. Chilkoti, Plasmonic detection of a model analyte in serum by a gold nanorod sensor. *Anal. Chem.* **79**, 5278-5283 (2007).
4. A. Tronin, Y. Lvov, C. Nicolini, Ellipsometry and X-ray reflectometry characterization of self-assembly process of polystyrenesulfonate and polyallylamine. *Colloid Polym. Sci.* **272**, 1317-1321 (1994).

5. N. Cant *et al.*, Fabrication and characterization of self-assembled nanoparticle/polyelectrolyte multilayer films. *J. Phys. Chem. B* **107**, 13557-13562 (2003).
6. Huang, F. M., Wilding, D, Speed, J. D., Russell, A. E., Bartlett, P. N., Baumberg, J. J., Dressing plasmons in particle-in-cavity architectures. *NanoLetters* **2011***, 11*, 1221-1226.
7. Harris, J. J. &Bruening, M. L. *Langmuir* **16**, 2006-2013 (2000).
8. Wong, J. E., Rehfeldt, F., Hanni, P., Tanaka, M., & Klitzing, R. V. *Macromolecules* **37**, 7285-7289 (2004).
9. Kugler, R., Schmitt, J., & Knoll, W. *Macromol. Chem. Phys.* **203**, 413-419 (2002).
10. Losche, M., Schmitt, J., Decher, G., Bouwman, W. G., &Kjaer, K. *Macromolecules* **31**, 8893-8906 (1998).